A water retention model accounting for the hysteresis induced by hydraulic and mechanical wetting-drying cycles

Arash Azizi[1,4*], Cristina Jommi[2] and Guido Musso[3]

*Corresponding author

1. Ph.D. Researcher

Department of Civil and Environmental Engineering

Politecnico di Milano

Piazza Leonardo da Vinci, 32

20133 Milano, Italy

arash.azizi@polimi.it

2. Professor

Department of Geoscience and Engineering

Delft University of Technology

Stevinweg, 1

2628 CN Delft, The Netherlands

c.jommi@tudelft.nl

3. Associate Professor

Department of Structural, Geotechnical and Building Engineering

Politecnico di Torino

Corso Duca degli Abruzzi, 24

10129 Torino, Italy

guido.musso@polito.it

4. Post-doc Researcher (current position)

Department of Structural, Geotechnical and Building Engineering

Politecnico di Torino

Corso Duca degli Abruzzi, 24

10129 Torino, Italy

arash.azizi@polito.it

ABSTRACT

A comprehensive description of the water retention behaviour of unsaturated soils requires accounting for the hysteresis caused by hydraulic and mechanical wetting-drying cycles. A hysteretic water retention model is proposed by introducing the liquid-solid contact angle to account for the dependency of the response on non-monotonic changes in suction and void ratio. The proposed model reproduces main drying and wetting surfaces and also nonlinear scanning curves during hydraulic or mechanical loading. Experimental tests and numerical simulations were carried out to study the water retention behaviour of a clayey silt. The model simulations captured the experimental results well.

Key words: soil water retention; hysteresis; suction; contact angle

Number of words: 6952
Number of figures: 10
Number of tables: 2
Number of appendixes: 2

1. INTRODUCTION

The behaviour of unsaturated soils and its modelling are more complicated than those of saturated soils, not only because of the complex role of suction but also due to the fact that the relationship between suction and water content depends on several factors. Among them are the structure and porosity of the soil, which descend from its history, and the direction of the hydraulic path – i.e. wetting or drying. An accurate description of water retention is needed for modelling both two-phase flow and mechanical behaviour, and advanced constitutive models explicitly require information related to water content or degree of saturation (e.g. Jommi, 2000; Tamagnini, 2004; Sun et al., 2007; Romero and Jommi, 2008; Della Vecchia et al., 2013; Zhou and Sheng 2015).

In the present paper, some existing water retention models are briefly discussed before introducing the concept of contact angle hysteresis which describes changes in the contractile skin (the air-water interface formed between soil particles) during wetting-drying and compression-swelling processes. The concept is implemented to develop a water retention model (WRM) which accounts for the hysteresis induced by changes in soil suction (hydraulic wetting-drying) and changes in soil volume (compression-swelling or mechanical wetting-drying).

Experimental tests were carried out to study the water retention behaviour of a clayey silt during hydraulic and mechanical wetting-drying cycles, and the proposed model was employed to predict the experimental data. The experimental results showed a hysteretic behaviour which was well predicted by the model.

1.1 SOIL WATER RETENTION

The relationship between the amount of water stored within pores of unsaturated soils and suction (s) is known as the water retention curve. Different variables are used to describe the quantity of stored water: e.g. gravimetric water content (w), volumetric water content (θ), degree of saturation (S_r). First proposals of water retention models (e.g. Gardner, 1958; Brooks and Corey, 1964; Campbell, 1974; van Genuchten, 1980; Fredlund and Xing, 1994) introduced a unique relationship

between the amount of stored water (represented by S_r in this paper) and suction, which can be written as:

$$S_r = \Gamma(s) \tag{1}$$

where Γ is a function relating suction to degree of saturation.

These models are simple and empirical but well applicable expressions which allow the model to fit the experimental data with a limited number of parameters. However, the hysteresis associated with drying and wetting of the soil ascertained that there is no unique soil water retention curve. There are numbers of transitional drying and wetting scanning curves bounded between the main drying and main wetting curves. These scanning curves become asymptotic to the main bounding curves. Numerous models have been developed accounting for the hysteresis of soil water retention using the one-dimensional elastoplastic framework in a way that the elastic (scanning) domain is bounded by the main curves, which act as yielding limits in the S_r-s plane (e.g. Vaunat et al., 2000; Wheeler et al., 2003; Tamagnini, 2004; Nuth and Laloui, 2008; Sheng and Zhou, 2011). Recent water retention models have been formulated with differential equations, which provide more capability to capture smooth nonlinear scanning curves without distinction between elastic and plastic zones (e.g. Li, 2005; Pedroso and Williams, 2010; Liu et al., 2012; Zhou et al., 2012; Tsiampousi et al., 2013). These models may be formulated in a rate form as below,

$$\dot{S_r} = \Gamma(s, \dot{s}) \tag{2}$$

Furthermore, the water retention behaviour depends also on mechanical variables (e.g. soil density or void ratio, volumetric strain, stress variable). Any change in these variables influences the amount of stored water, particularly in the low suction range, resulting mainly in changes in the air-entry value of the drying water retention curve or the air-occlusion value of the wetting water retention curve (e.g. Vanapalli et al., 1999; Romero and Vaunat, 2000; Ng and Pang, 2000; Miller et al. 2002; Tarantino and Tombolato, 2005). Models have been proposed accounting for these effects (e.g. Gallipoli et al., 2003; Sun et al., 2007; Nuth and Laloui, 2008; Tarantino, 2009; Mašín,

2010; Zhou et al., 2012); they can be written as:

$$S_r = \Gamma(s, \xi) \tag{3}$$

where ξ is a mechanical variable.

The mechanical dependency and the hysteresis of water retention indicated that the main drying and main wetting curves of deformable soils can be characterized by two surfaces in the S_r-s-ξ space, namely, the main drying surface and the main wetting surface (e.g. Tarantino et al., 2008; Salager et al., 2010, Gallipoli et al., 2012), as shown in Figure 1, where the mechanical variable is assumed to be the void ratio (e). The intersection of the main drying and wetting surfaces with the S_r-e plane at constant suction represents the main compression curve and the main swelling curve, respectively. On the other hand, the intersections with the S_r-s plane at constant void ratio represent the main wetting curve and the main drying curve.

Gallipoli et al., (2003) proposed a model which accounts for the mechanical dependency of the water retention behaviour by explicitly incorporating the effect of void ratio on the air-entry value, in which the degree of saturation can be computed depending on suction and void ratio,

$$S_r = \Gamma(s, e) = [1 + (ae^{\alpha}s)^n]^{-m} \tag{4}$$

where n and m are parameters of the van Genuchten (1980) model, and a and α are two additional parameters which introduce the dependency of the air-entry value on the void ratio. Therefore, the model can reproduce the main drying or main wetting curve (depending on which water retention curve the van Genuchten parameters are calibrated) and also the main compression curve. This results in the definition of a water retention surface in the S_r-s-e space, which allows the model to predict irreversible changes of degree of saturation due to irreversible changes of void ratio. However, this model is not appropriate for problems involving significant hysteresis since the latter is not taken into account.
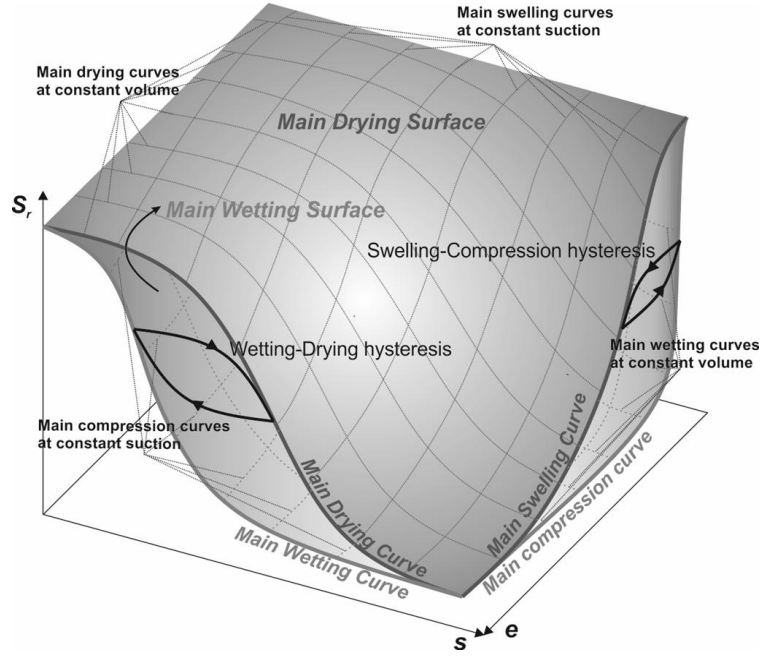
Figure 1. Main drying and wetting surfaces and hysteresis induced by hydraulic and mechanical wetting-drying cycles.

A general rate form expression for a WRM, which allows to account for mechanical dependency and hydraulic hysteresis, is:

$$\dot{S}_r = \Gamma(s, \dot{s}, \xi) \tag{5}$$

According to the most existing rate form WRMs, the scanning curves can be predicted by a data-fitting methodology, using the interpolation between the projections of suction or degree of saturation on the main drying and main wetting branches. These water retention models have been commonly derived by applying the capillary law to the cumulative distribution function of soil pores while the contact angle was assumed to be constant. Zhou (2013) proposed a contact angle-dependent WRM interpreting the hydraulic hysteresis in terms of contact angle hysteresis. The proposed contact angle-dependent WRM also adopted the van Genuchten (1980) model to reproduce the main drying curve, whereas scanning and main wetting curves were predicted depending on the variation of contact angle. The model employs a single function including two incremental terms. The first one describes the direct change in the effective degree of saturation ($\dot{S}_e$) due to suction changes, and the second one stands for the variation of the effective degree of saturation associated with the contact angle change ($\dot{\theta}$) induced by suction changes.

6

$$\dot{S}_e = \Gamma(s,\theta) = \frac{\partial S_e}{\partial s}\dot{s} + \frac{\partial S_e}{\partial \theta}\dot{\theta} \qquad (6)$$

This model was developed assuming that the value of the contact angle remains the lowest possible along the whole main drying water retention curve whereas it keeps its highest value along the whole main wetting water retention curve. Therefore, scanning curves were reproduced by changing the contact angle between its minimum and maximum limits. However, the mechanical dependency of the water retention behaviour was neglected in the model.

When matric suction is kept constant, loading and unloading induce an irreversible change in the degree of saturation. This implies that the hydraulic hysteresis is not only associated with the change in suction but also it can be induced by the volume change of the soil sample. Therefore, a hysteretic WRM should be able to take into account the hysteresis caused by wetting-drying cycles at constant volume and also the hysteresis caused by compression-swelling cycles at constant suction. However, only a few models have considered the latter case (e.g. Khalili et al., 2008; Nuth & Laloui, 2008; Tarantino, 2009; Gallipoli, 2012).

1.2 CONTACT ANGLE HYSTERESIS

As discussed by Hillel (1998), the hydraulic hysteresis may be caused by a combination of different phenomena at the pore scale: non-uniformity of pores which is known as "ink-bottle" effect; air entrapped in irregularly shaped pores; volume changes; and contact angle hysteresis. Although a predominant effect has not been recognised, a pragmatic choice for the model formulation is to ascribe the hysteresis to a single phenomenon, to keep the number of parameters of the model limited. The contact angle hysteresis has been chosen for this purpose by several authors (e.g. Song et al., 2012; Diamantopoulos et al., 2013; Zhou, 2013; Gan et al., 2013).

The contact angle (θ) is defined as the angle formed by the intersection of the liquid-solid and the liquid-vapour interfaces within the soil mass. The contact angle takes values between the maximum contact angle (advancing, θ_A) and minimum contact angle (receding, θ_R), and the difference between θ_A and θ_R is known as the contact angle hysteresis (e.g. Johnson and Dettre, 1964;

Schwartz and Garoff, 1985; Gao and McCarthy, 2006; Krumpfer and McCarthy, 2010). The contact angle hysteresis consists of two components: static and dynamic hysteresis. According to Rotenberg et al. (1984), dynamic hysteresis can be neglected for a slow-moving liquid on rough solid surfaces (e.g. soil particles). Therefore, static hysteresis is the dominant component under this condition which arises from surface roughness and heterogeneity (Johnson and Dettre, 1964).

Figure 2 shows two hypothetical spherical soil particles linked by a water bridge while being subjected to drying, wetting, compression, and swelling. The hydraulic wetting and drying processes are displayed by means of changes in the water meniscus while the position of the soil particles remains fixed. When the amount of water increases during wetting, the position of the water meniscus initially remains unchanged and the contact angle increases. Once the contact angle reaches the advancing contact angle ($\theta=\theta_A$), the water meniscus starts moving upward while the contact angle remains constant (Figure 2 (a)). In contrast, when the amount of water decreases during drying, the contact angle initially reduces to the receding contact angle ($\theta=\theta_R$). Upon further drying, the contact angle remains constant and the water meniscus starts moving downward (Figure 2 (b)). The process in which the contact angle changes while the position of the water meniscus remains unchanged is called pinning. The process in which the water meniscus moves while the contact angle remains constant is known as slipping. Similarly, pinning and slipping occur when the soil volume changes during compression and swelling. Compression and swelling can be replicated by bringing the soil particles closer together (Figure 2 (c)) or moving them apart (Figure 2 (d)), respectively. When the soil volume decreases (mechanical wetting), θ increases to θ_A, followed by slipping while θ remains equal to θ_A for further compression. On the other hand, when the soil volume increases (mechanical drying), θ decreases to θ_R, followed by slipping while θ remains equal to θ_R for further swelling.

Experimental evidence of such irreversible changes in the contact angle was reported looking into the behaviour of a liquid bridge being compressed and stretched between two solid surfaces (Fortes, 1982; Hong et al., 2012; Longley et al. 2012, Chen et al., 2014). The results showed that the contact

line can expand or shrink, or remain pinned during compressing and stretching the liquid bridge while the contact angles at the surfaces can change between their advancing and receding values (for details see Appendix A).
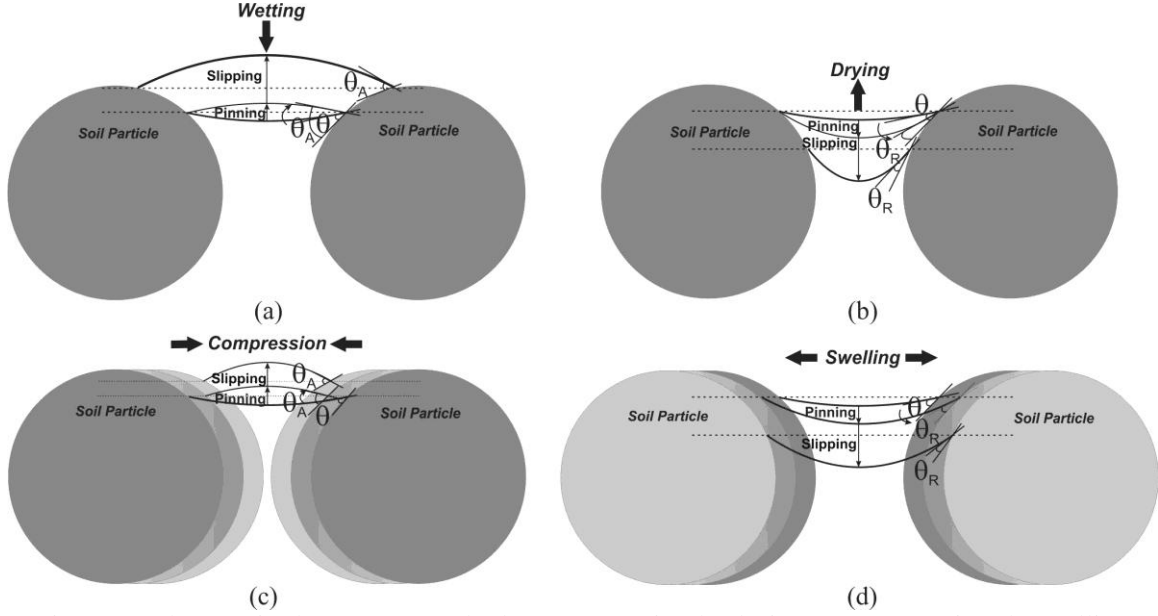

Figure 2. Changes in the contact angle due to a) wetting b) drying c) compression d) swelling.

The water retention behaviour during wetting-drying and compression-swelling, together with corresponding changes in the contact angle, are represented in Figures 3 (a) and 3 (b). The contact angle changes between θ_R and θ_A (pinning) during hydraulic and mechanical wetting-drying when the hydraulic state lies in the scanning domain, but it remains equal to θ_A (slipping) during wetting or compression upon the main wetting surface and it remains equal to θ_R (slipping) during drying or swelling upon the main drying surface.
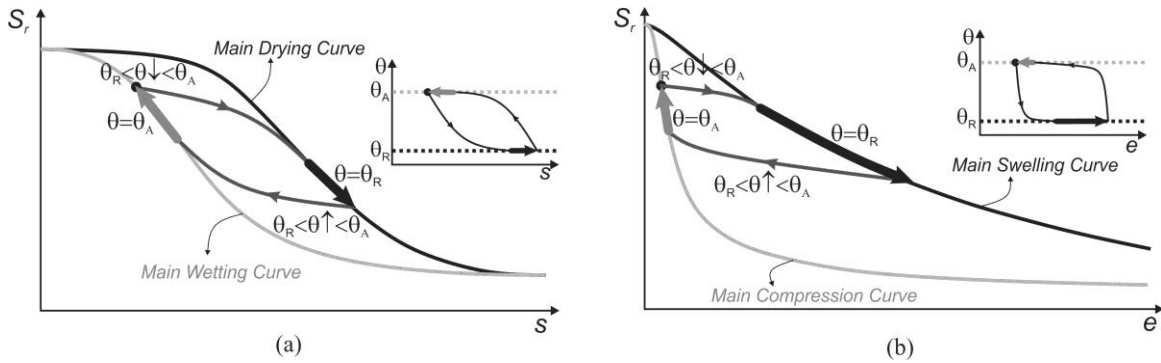

Figure 3. Water retention behaviour and corresponding changes in the contact angle
(a) drying and wetting in S_r-$\log s$ plane (b) compression and swelling in S_r-e plane.

In the following, a hysteretic WRM is proposed incorporating the dependency of the contact angle and water retention on void ratio and suction. The contact angle approach (Zhou 2013) was integrated into the WRM proposed by Gallipoli (2003), which was adopted as the reference model. The rate form equation was derived introducing two hysteresis functions, which control the hysteresis of water retention induced by wetting-drying and compression-swelling cycles.

2. A HYSTERETIC WATER RETENTION MODEL FOR DEFORMABLE SOILS

The cumulative function $(F(R))$ measures the amount of pores having the radius smaller than any arbitrary radius R, and it can be derived by integrating the pore size distribution $(f(r))$ between the minimum radius (R_{min}) and R,

$$F(R) = \int_{R_{min}}^{R} f(r)dr \tag{7}$$

If the geometry of the pore network of unsaturated soils is simplified assuming different cylindrical tubes having different sizes, the different pores are assumed to be sequentially filled starting from the smallest one during a wetting process. The current degree of saturation $(S_r(R))$ can be then identified if the pores between R_{min} and R are filled with water,

$$S_r(R) = \int_{R_{min}}^{R} f(r)dr = F(R) \tag{8}$$

The arbitrary pore radius R can be obtained by the inverse of the cumulative function,

$$R = F^{-1}(S_r(R)) \tag{9}$$

For a given degree of saturation, the capillary law can be used to relate an arbitrary suction (s) to the suction on the main drying surface (s_d):

$$s = \frac{2\sigma \cos\theta}{R} = \frac{2\sigma \cos\theta}{F^{-1}(S_r(R))} \tag{10}$$

and,

$$s_d = \frac{2\sigma \cos\theta_R}{R} = \frac{2\sigma \cos\theta_R}{F^{-1}(S_r(R))} \tag{11}$$

10

where the contact angles for s and s_d are θ and θ_R, respectively.

Comparing Eqs. (10) and (11) gives a relationship between s and s_d (Zhou, 2013),

$$s_d = \frac{s\cos\theta_R}{\cos\theta} \tag{12}$$

The WRM proposed by Gallipoli (2003) is adopted as the reference model, which can be written as below (according to Eq. (4)),

$$S_r = [1 + (ae^\alpha s_d)^n]^{-m} \tag{13}$$

where $s=s_d$ for the main drying curve.

If s_d is replaced according to Eq. (12),

$$S_r = \left[1 + \left(\frac{ae^\alpha s\cos\theta_R}{\cos\theta}\right)^n\right]^{-m} \tag{14}$$

The incremental form of Eq. (14) can be obtained by differentiation with respect to s, e and θ, which explicitly shows the changes in the degree of saturation ($\dot{S}_r$) induced by changes in suction ($\dot{s}$), void ratio ($\dot{e}$) and contact angle ($\dot{\theta}$),

$$\dot{S}_r = \frac{\partial S_r}{\partial s}\dot{s} + \frac{\partial S_r}{\partial e}\dot{e} + \frac{\partial S_r}{\partial \theta}\dot{\theta} \tag{15}$$

Differentiation of Eq. (14) gives:

$$\frac{\partial S_r}{\partial s} = -\frac{mn}{s}\left(\frac{ae^\alpha s\cos\theta_R}{\cos\theta}\right)^n\left[1 + \left(\frac{ae^\alpha s\cos\theta_R}{\cos\theta}\right)^n\right]^{-m-1} = \frac{\phi}{s} \tag{16}$$

$$\frac{\partial S_r}{\partial e} = -\frac{mn\alpha}{e}\left(\frac{ae^\alpha s\cos\theta_R}{\cos\theta}\right)^n\left[1 + \left(\frac{ae^\alpha s\cos\theta_R}{\cos\theta}\right)^n\right]^{-m-1} = \alpha\frac{\phi}{e} \tag{17}$$

$$\frac{\partial S_r}{\partial \theta} = -mn\tan\theta\left(\frac{ae^\alpha s\cos\theta_R}{\cos\theta}\right)^n\left[1 + \left(\frac{ae^\alpha s\cos\theta_R}{\cos\theta}\right)^n\right]^{-m-1} = \phi\tan\theta \tag{18}$$

where ϕ is defined as $\phi = -mn(\frac{ae^\alpha s\cos\theta_R}{\cos\theta})^n\left[1 + (\frac{ae^\alpha s\cos\theta_R}{\cos\theta})^n\right]^{-m-1}$ for simplification.

Hence, the incremental form of the degree of saturation can be rewritten as:

$$\dot{S}_r = \frac{\phi}{s}\dot{s} + \alpha\frac{\phi}{e}\dot{e} + \phi\tan\theta\,\dot{\theta} \tag{19}$$

11

where the contact angle changes with suction and void ratio,

$$\dot{\theta} = \frac{\partial \theta}{\partial s} \dot{s} + \frac{\partial \theta}{\partial e} \dot{e} \tag{20}$$

Eq. (15) can be then rearranged in the form:

$$\dot{S}_r = (\frac{\partial S_r}{\partial s} + \frac{\partial S_r}{\partial \theta} \frac{\partial \theta}{\partial s}) \dot{s} + (\frac{\partial S_r}{\partial e} + \frac{\partial S_r}{\partial \theta} \frac{\partial \theta}{\partial e}) \dot{e} \tag{21}$$

Substituting Eqs. (16), (17) and (18) into Eq. (21) yields:

$$\dot{S}_r = \frac{\phi}{s} \left[1 + \frac{\partial \theta}{\partial s} s \tan \theta \right] \dot{s} + \alpha \frac{\phi}{e} \left[1 + \frac{\partial \theta}{\partial e} \frac{e \tan \theta}{\alpha} \right] \dot{e} \tag{22}$$

The first term of Eq. (22) contributes to the change in the degree of saturation when suction changes, in which $\frac{\partial \theta}{\partial s} s \tan \theta$ is employed to reproduce the hysteresis during hydraulic wetting-drying cycles. The second term of Eq. (22) accounts for the effect of void ratio on the variation of the degree of saturation, and the hysteresis during compression-swelling cycles is introduced by $\frac{\partial \theta}{\partial e} \frac{e \tan \theta}{\alpha}$. If the derivatives of the contact angle with respect to suction and void ratio take the form:

$$\frac{\partial \theta}{\partial s} = -H_\theta{}^s (\frac{1}{s \tan \theta}) \tag{23}$$

and,

$$\frac{\partial \theta}{\partial e} = -H_\theta{}^e (\frac{\alpha}{e \tan \theta}) \tag{24}$$

where the hydraulic hysteresis function ($H_\theta{}^s$) and the mechanical hysteresis function ($H_\theta{}^e$) are incorporated to model the hysteresis of water retention due to changes in suction and void ratio, respectively, Eq. (22) can be rewritten as:

$$\dot{S}_r = \frac{\phi}{s} [1 - H_\theta{}^s] \dot{s} + \alpha \frac{\phi}{e} [1 - H_\theta{}^e] \dot{e} \tag{25}$$

When the hysteresis functions (H_θ) are 0, the variation of the contact angle does not contribute to changes in the degree of saturation ($\dot{\theta}$=0). This implies that the water retention curve lies on the main wetting or drying surfaces where the contact angle is θ_A or θ_R, respectively. Moreover, Eq.

(25) predicts no changes in the degree of saturation if the hysteresis functions are 1. Hence, changes in the degree of saturation are declined by the variation of the contact angle as the hysteresis functions decrease from 1 to 0 during wetting-drying or compression-swelling processes, resulting in reproducing smooth nonlinear scanning curves as shown in Figure 4. It means that the hysteresis functions can be defined in such a way that their value remains 0 on the main wetting and drying surfaces whereas they shift to 1 at any turning point, where either wetting (or compression) occurs on the main drying surface or drying (or swelling) occurs on the main wetting surface. When the contact angle is θ_R on the main drying branch, the water retention curve lies on the main drying surface for the following swelling process. Hence, the hysteresis functions are not employed since swelling affects the contact angle in the same way as the drying process does. However, the water retention state moves toward the main wetting surface if compression occurs, so the contact angle increases from θ_R to θ_A and $H_\theta{}^e$ shifts from 0 to 1. When the initial hydraulic state lies on the main wetting branch, the opposite occurs. Accordingly, the hysteresis functions can take the same mathematical form for drying and swelling or wetting and compression.
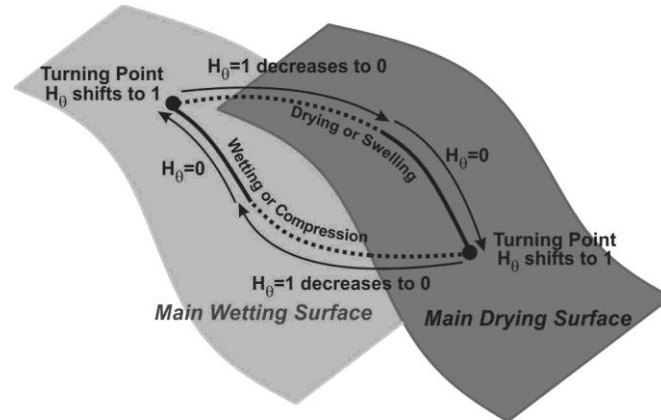

Figure 4. Evolution of hysteresis functions during wetting-drying and compression-swelling.

A physical model for the hysteresis functions based on the geometrical-mechanical relationship between soil particles and connected water bridges would be desirable. However, simple logarithmic equations are hereby proposed for the aim of simplicity having the same shape for drying and swelling, and for wetting and compression:

$$H_\theta{}^s = \left[\frac{\log\left(\frac{\cos\theta}{\cos\theta_R}\right)}{\log\left(\frac{\cos\theta_A}{\cos\theta_R}\right)}\right]^{\beta_s}, \dot{s} > 0 \;\; \text{and} \;\; H_\theta{}^e = \left[\frac{\log\left(\frac{\cos\theta}{\cos\theta_R}\right)}{\log\left(\frac{\cos\theta_A}{\cos\theta_R}\right)}\right]^{\beta_e}, \dot{e} > 0 \tag{26}$$

$$H_\theta{}^s = \left[\frac{\log\left(\frac{\cos\theta_A}{\cos\theta}\right)}{\log\left(\frac{\cos\theta_A}{\cos\theta_R}\right)}\right]^{\beta_s}, \dot{s} < 0 \;\; \text{and} \;\; H_\theta{}^e = \left[\frac{\log\left(\frac{\cos\theta_A}{\cos\theta}\right)}{\log\left(\frac{\cos\theta_A}{\cos\theta_R}\right)}\right]^{\beta_e}, \dot{e} < 0 \tag{27}$$

where β_s and β_e are model parameters.

It is worthwhile pointing out that such a model can be represented in a rate form as:

$$\dot{S}_r = \Gamma(s, e, \theta, \dot{\theta}) \tag{28}$$

where changes in the contact angle depend on changes in suction and void ratio,

$$\dot{\theta} = Y(\dot{s}, \dot{e}) \tag{29}$$

where Y is a function relating changes in the contact angle to changes in suction and void ratio.

3. PARAMETERS CALIBRATION

The parameters of the adopted reference model (n, m, α, a) can be calibrated by performing a best fitting least-square procedure, in the S_r-s-e space, on the parameters for the main drying and the main compression curves. As proposed by van Genuchten (1980), the number of independent parameters can be reduced by fixing m as a function of n,

$$m = 1 - \frac{1}{n} \tag{30}$$

Together, Eqs. (23) and (24) show that the contact angle varies in a domain between two horizontal planes formed by θ_A and θ_R in the θ-s-e space. The contact angle lies on the upper plane ($\theta=\theta_A$) when the water retention curve rests on the main wetting surface, and it lies on the lower plane ($\theta=\theta_R$) when the water retention curve rests on the main drying surface, while it varies between these two planes when hydraulic states are represented by scanning curves.

For most soils θ_R is very low and it can be assumed to be null (e.g. Ethington, 1990; Bachmann et al., 2003; Shang et al., 2008), which reduces the number of unknown parameters (Zhou, 2013). The

advancing contact angle, θ_A, can be calibrated using the main wetting curve and it controls the position of the main wetting surface. The proposed model predicts the wetting branch by incorporating the effect of changes in the contact angle on the air-entry value of the drying branch (for details see Appendix B). Thus, the air-entry value (ω_{ae}), and the air-occlusion value (ω_{ao}) can be used to provide an initial estimation of θ_A:

$$\theta_A = Arccos(\frac{\omega_{ao}}{\omega_{ae}}) \tag{31}$$

Further calibration by a best-fitting approach can improve the initial estimation.

The water retention behaviour of Viadana silt was investigated in the present research and the experimental results were compared to model predictions. For the tested soil ω_{ae} and ω_{ao} were detected to be 44 kPa and 5.5 kPa, respectively, and Eq. (31) gave θ_A equal to 82.8 degrees, which adequately predicted the main wetting surface of the water retention test results.

The parameters β_s and β_e control the rate of the contact angle variation, and in turn, govern the curvature of the scanning curve in the S_r-s and S_r-e planes. β_s can be calibrated using a scanning curve resulting from changes in suction at constant volume, and β_e from loading-unloading at constant suction. It was found that good accuracy in the reproduction of both wetting-drying and compression-swelling cycles could be obtained using the same value for both parameters ($\beta_s=\beta_e=\beta$). Eventually, only five parameters listed in Table 1 were employed to predict the experimental results. Nonetheless, the model was able to nicely predict the soil water retention behaviour in the S_r-s-e space including the main curves, nonlinear scanning curves and the hysteresis induced by compression-swelling and wetting-drying cycles.

Table 1. Parameters of the proposed model for Viadana silt.

Parameters	n	a	α	θ_A	β
Viadana silt	1.38	0.12	5.12	82.8	0.42

4. EXPERIMENTAL PROGRAMME

Oedometer tests were carried out to study the hysteresis of the soil water retention behaviour and to evaluate the predictive capability of the proposed WRM. The description of the experimental tests is presented in Table 2. The Oe-WR test was performed to obtain the main drying and main wetting curves by means of changing suction at constant axial net stress. The Oe-LU test was carried out to detect the main compression curve where the axial net stress increased at constant suction. Scanning curves were also detected while applying wetting-drying and loading-unloading cycles. The parameters of the model were calibrated using the experimental behaviour observed in these two tests. Two other tests (Oe-DW and Oe-LU-CW) were performed starting from different void ratios and applying different load paths. The parameters obtained from the previous calibration were introduced in the model to simulate these last two load paths, leading to blind predications that were compared to the experimental results.

The sample of the Oe-DW test was prepared at a lower density (higher porosity) compared to the one of the Oe-WR test. The experimental result and numerical simulation of the Oe-DW test showed the capability of the model to predict the water retention behaviour when volume changes (changes in void ratio) considerably contribute to changes in the degree of saturation during wetting-drying cycles. In the last test (Oe-LU-CW), the sample was subjected to loading-unloading cycles at constant water content while suction was measured. The model was then employed to predict suction at changing void ratio and degree of saturation.

It has to be pointed out that the experimental values of void ratio were adopted in the simulations, instead of predicting them from a coupled mechanical model. This choice was dictated by two main reasons: (a) ideally, the formulation should serve any mechanical counterpart, able to provide an estimation of the change in void ratio as a function of suction and degree of saturation, and (b) the use of a mechanical model to predict the change in void ratio, instead of directly using experimental data for void ratio, would hinder a detailed analysis of the approximation resulting from the water retention part on the prediction of the coupled response. However, the implementation of the

proposed model in geotechnical practice needs coupling with a mechanical counterpart (see e.g. Azizi, 2016).

Table 2. Description of the experimental tests.

Test title	Initial condition				Loading path		
	s kPa	σ_{v-net} kPa	e	S_r	s kPa	σ_{v-net} kPa	Water content
Oe-WR	10	50	0.62	1.00	10→350→10 →92000→10	Constant	Evolving
Oe-LU	50	10	0.97	0.52	Constant	10→600→10 →1600→10	Evolving
Oe-DW	400	10	0.93	0.30	400→10→400→5	Constant	Evolving
Oe-LU-CW	200	10	0.91	0.36	Measured	10→150→10→ 500→10→1500→10	Constant

4.1 TESTED MATERIAL AND SAMPLE PREPARATION

The soil used in the experimental study is a clayey silt, called "Viadana silt". Its silt fraction is 79.6%, whereas the clay fraction is 20.4%. The grain specific gravity (G_s), liquid limit (w_l) and plasticity index (PI) were found to be 2.73, 32.6% and 8.3%, respectively.

All samples were prepared using the static compaction technique. First, the dry soil powder was hand-mixed with demineralized water to reach the target water content. It was then sealed in a plastic bag and placed in a humid container for 48 hours allowing for water content equilibration. Next, the moist powder was placed in a hermetic mould with a diameter of 50 mm where it was compacted at constant water content by gradually increasing the axial force until the desired height of the specimen (20 mm) was achieved.

4.2 EXPERIMENTAL EQUIPMENT AND TECHNIQUES

The suction-controlled oedometer and axis translation technique were used to perform tests in which imposed and measured suction was smaller than 400 kPa. The vapour equilibrium technique was also used to study the water retention behaviour for s>4 MPa. In the latter case, the sample was placed in a closed desiccator and supported above a saturated saline solution. Different saturated solutions were used to control the air relative humidity (RH) in the closed desiccator. The weight

and the size of the sample were frequently measured. About one month was needed to achieve water content equilibrium under specified RH. The used saturated solutions (and corresponding suction as reported by Romero (2001)) were K_2SO4 (4 MPa), KNO_3 (11 MPa), KCl (24 MPa), $NaNO_3$ (41 MPa) and $Ca(NO_3)\cdot4H_2O$ (92 MPa).

5. EXPERIMENTAL RESULTS AND MODEL VALIDATION

5.1 TEST Oe-WR AND MODEL PREDICTIONS

Figure 5 shows the experimental result of the Oe-WR test compared to the model predictions. The sample was compacted at a water content of 20.2% and a dry density of 1650 kg/m^3 (corresponding to e_0=0.66 and S_{r0}=0.84), and it was then placed in the oedometer and subjected to an axial net stress σ_{v-net}=50 kPa and an initial suction s=10 kPa. The water retention behaviour was studied by increasing the suction to 350 kPa, followed by a wetting-drying cycle where the suction decreased to 10 kPa and then increased to 400 kPa. The sample was then unloaded, removed from the oedometer and eventually placed in the desiccator. An axial net stress of σ_{v-net}=20 kPa was applied by means of a dead weight placed above the sample. The void ratio change recorded during unloading and subsequent reloading was very small (see Figure 5 (b)), hence it was assumed to have no influence on the hydraulic response. In the desiccator, the sample was subjected to drying followed by wetting. The wetting path continued by placing back the sample in the oedometer and decreasing the suction from 400 kPa to 10 kPa. The applied loading path is shown in Figure 5 (a). Figure 5 (b) shows that the sample experienced insignificant and mainly reversible volume changes during the wetting-drying paths. The main drying and wetting curves and also two scanning curves were detected (Figure 5 (c)).

As shown in Figure 5 (c), the proposed model was used to capture the experimental water retention behaviour. The experimental void ratio was adopted in the numerical computation and the degree of saturation was predicted. Figure 5 (d) shows the evolution of the contact angle with suction and void ratio during the wetting-drying cycles. The volume change of the sample was negligible, hence

the variation of the contact angle and the irreversible change of the degree of saturation mostly resulted from changes in suction. It can be observed that the contact angle was θ_R (lower plane) during the initial drying path, but the hysteresis induced by the first wetting-drying cycle was predicted by the variation of the contact angle, represented by the loop formed between the two planes (θ_R and θ_A) in Figure 5 (d). The contact angle remained on the lower plane during further drying. The degree of saturation at the maximum imposed suction, s=92 MPa, was very low (S_r=0.06). At the beginning of the subsequent wetting path, the contact angle increased and the point representing the state of the sample followed a scanning curve until θ reached θ_A at a suction of about 7000 kPa. From this point onward, the main wetting branch was followed, and the contact angle remained equal to θ_A (upper plane). The model was able to consistently predict the main wetting curve and the hysteresis of water retention by introducing the variation of the contact angle.
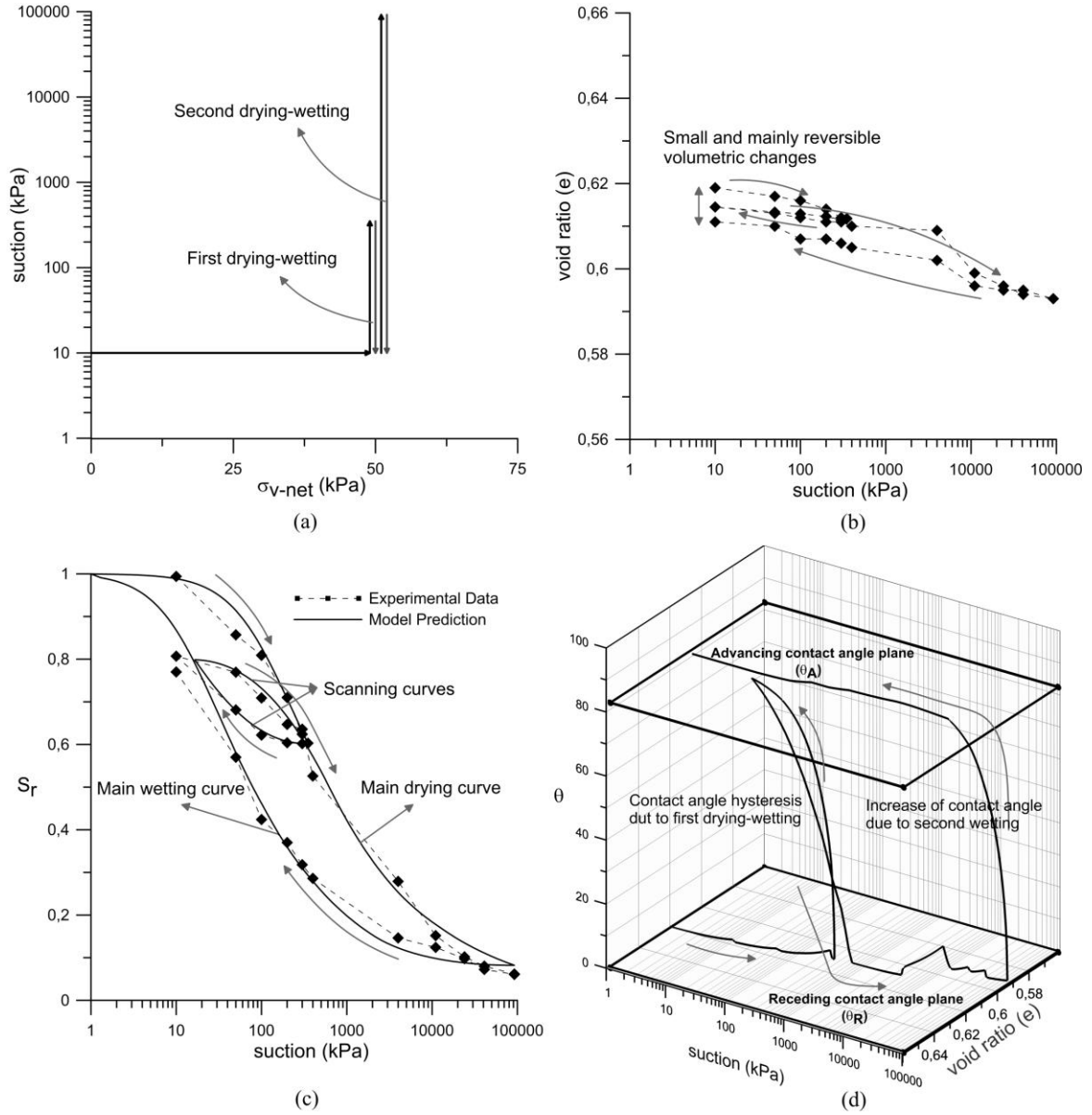
Figure 5. Computed and experimental behaviour during wetting–drying cycles at constant axial net stress (a) applied loading path (b) void ratio-suction data (c) degree of saturation-suction data and predictions (d) evolution of the contact angle with suction and void ratio.

5.2 TEST Oe-LU AND MODEL PREDICTIONS

Figure 6 presents the results of loading-unloading cycles at constant suction of 50 kPa (Oe-LU test). The sample was prepared at a dry density of 1370 kg/m^3 and a water content of 23.3% (corresponding to e_0=0.99 and S_{r0}=0.66). First, the sample was subjected to an initial suction s=50 kPa while the axial net stress was σ_{v-net}=10 kPa. The sample was initially dried and contracted due to the increase in suction from the post-compaction value to the imposed one. During the first loading-unloading cycle the axial net stress increased to σ_{v-net}=600 kPa and then decreased to

σ_{v-net}=10 kPa. During the second loading-unloading cycle the axial net stress increased from σ_{v-net}=10 kPa to σ_{v-net}=1600 kPa and it was then brought back to σ_{v-net}=10 kPa. The suction was kept constant at 50 kPa during both loading-unloading cycles (Figure 6 (a)). The void ratio decreased as the axial net stress increased (Figure 6 (b)), with a simultaneous increase of the degree of saturation (Figure 6 (c)). The increase in the degree of saturation was amplified as the water retention state approached the main compression curve for further volume reduction. On the other hand, the degree of saturation gently decreased due to volume expansion as it was being mechanically dried during unloading.

A mechanical hysteresis and an irreversible change of the degree of saturation occurred when the sample was subjected to the loading-unloading cycle (Figure 6 (c)). The predicted degree of saturation is also plotted in Figure 6 (c). It can be observed that the water retention lied in the scanning domain during the unloading-reloading cycle, which was predicted by the model. The contact angle is represented in Figure 6 (d) where it increased to θ_A during the first loading path, and the contact angle hysteresis induced by the unloading-reloading cycle can be appreciated.

The importance of the effect of the mechanical hysteresis depends on the range of loading-unloading and also on the mechanical response of the material. Although Viadana silt is not an expansive soil and the volume change experienced during unloading-reloading was limited, the mechanical hysteresis noticeably impacted on water retention. If $H_\theta{}^e$=0 were assumed, the model would predict the same curve for the compression and swelling paths, represented by the main compression curve in Figure 6 (c). Introducing the effect of hysteresis ($H_\theta{}^e \neq 0$) allows consuming a portion of $\dot{S}_r$ as a consequence of the variation of the contact angle due to changes in void ratio, which results in predicting irreversible changes in the degree of saturation. It can be appreciated that neglecting the effect of the hysteresis would result in underestimating the degree of saturation at the end of unloading, particularly for the second unloading path. This difference in S_r might cause relevant errors in the prediction of the hydromechanical behaviour of unsaturated soils since

both the mechanical and the hydraulic behaviour are dependent on S_r. Such evidence would be even more pronounced in the case of expansive soils.
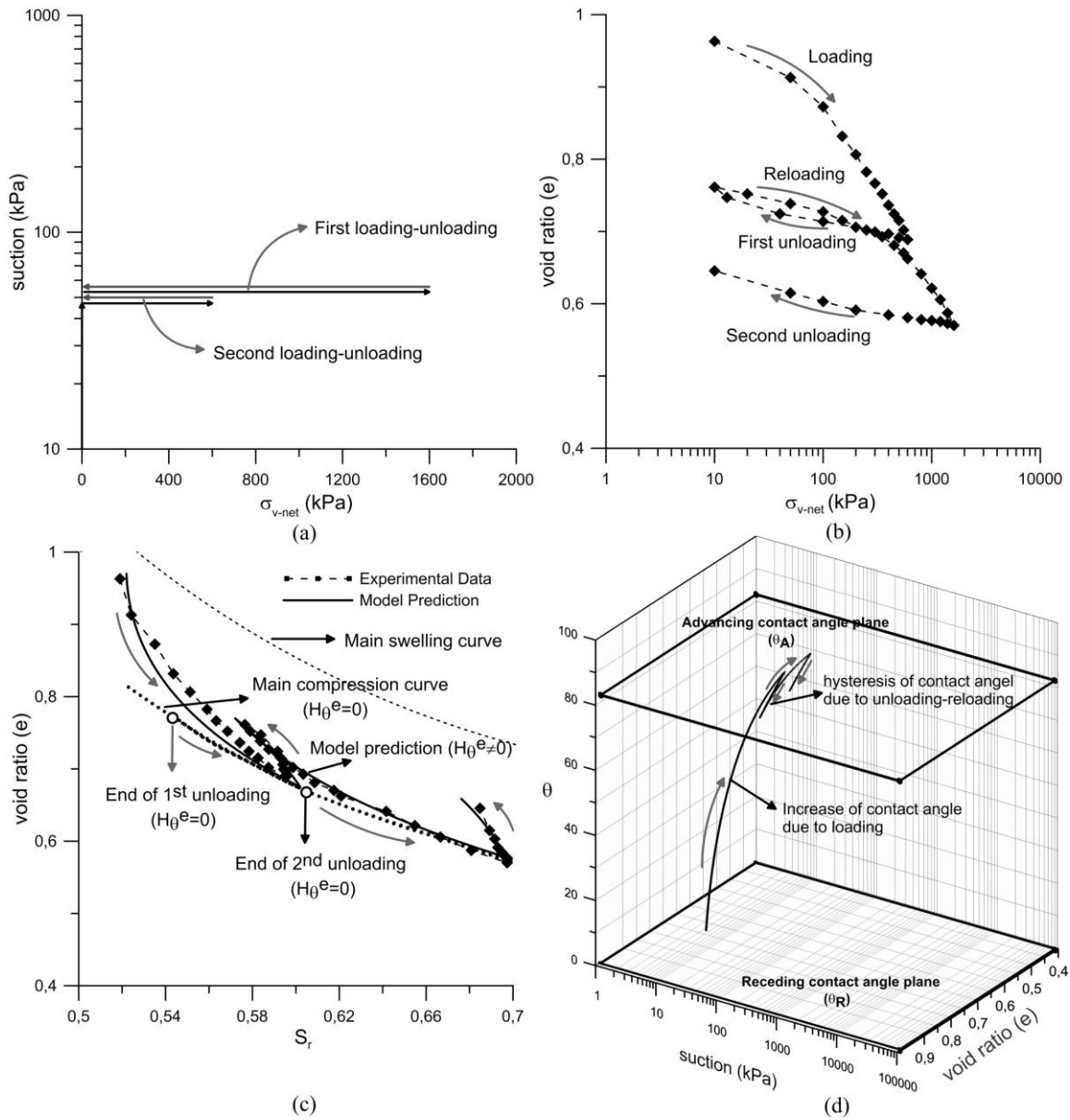

Figure 6. Computed and experimental behaviour during loading–unloading cycles at constant suction
(a) applied loading path (b) void ratio-net stress data (c) void ratio-degree of saturation data and predictions
(d) evolution of the contact angle with suction and void ratio.

5.3 TEST Oe-DW AND MODEL PREDICTIONS

In order to study the experimental behaviour and evaluate the model performance where both mechanical and hydraulic hysteresis considerably contribute to the water retention behaviour, two cycles of wetting-drying were applied to the loose sample while the axial net stress was kept constant at 10 kPa (Oe-DW test). The sample was prepared at a dry density of 1380 kg/m^3 and a

water content of 24.6% (corresponding to e_0=0.98 and S_{r0}=0.69). It was then placed in the oedometer and subjected to s=400 kPa. As shown in Figure 7 (a), the first cycle included wetting, i.e., decreasing the suction from s=400 kPa to s=10 kPa (A-B), followed by increasing suction to s=400 kPa (B-C). The second cycle included decreasing the suction to s=5 kPa (C-D) and then increasing to s=400 kPa (D-E). The sample experienced volume collapse during first wetting (A-B) whereas its volumetric change was mainly reversible when being subjected to the subsequent drying and wetting paths (Figure 7 (b)). Figure 7 (c) shows the measured and the predicted degree of saturation in the S_r-s-e space, in which the main drying and wetting curves varied during the wetting-drying cycles because of continuous changes in the void ratio. Figure 7 (d) shows the evolution of the contact angle in the θ-s-e space, indicating that the irreversible change of the contact angle allowed the model to properly capture the transition between the scanning domain and the main wetting surface, consistently with the experimental results. The degree of saturation increased in the scanning domain approaching the main wetting surface due to the volumetric collapse experienced by the sample during the first wetting path (A-B), as shown in Figure 7 (e). The hydraulic state approached the scanning domain as the sample was dried (B-C). The degree of saturation increased earlier during the second wetting path because of the smaller void ratio. This resulted in a shift of the main wetting curve to the upper position in the main wetting surface, while consequently the contact angle reached earlier the θ_A value. Figures 7 (e) and 7 (f) show the degree of saturation in terms of void ratio and suction, respectively. A very good reproduction of the experimental data was obtained.
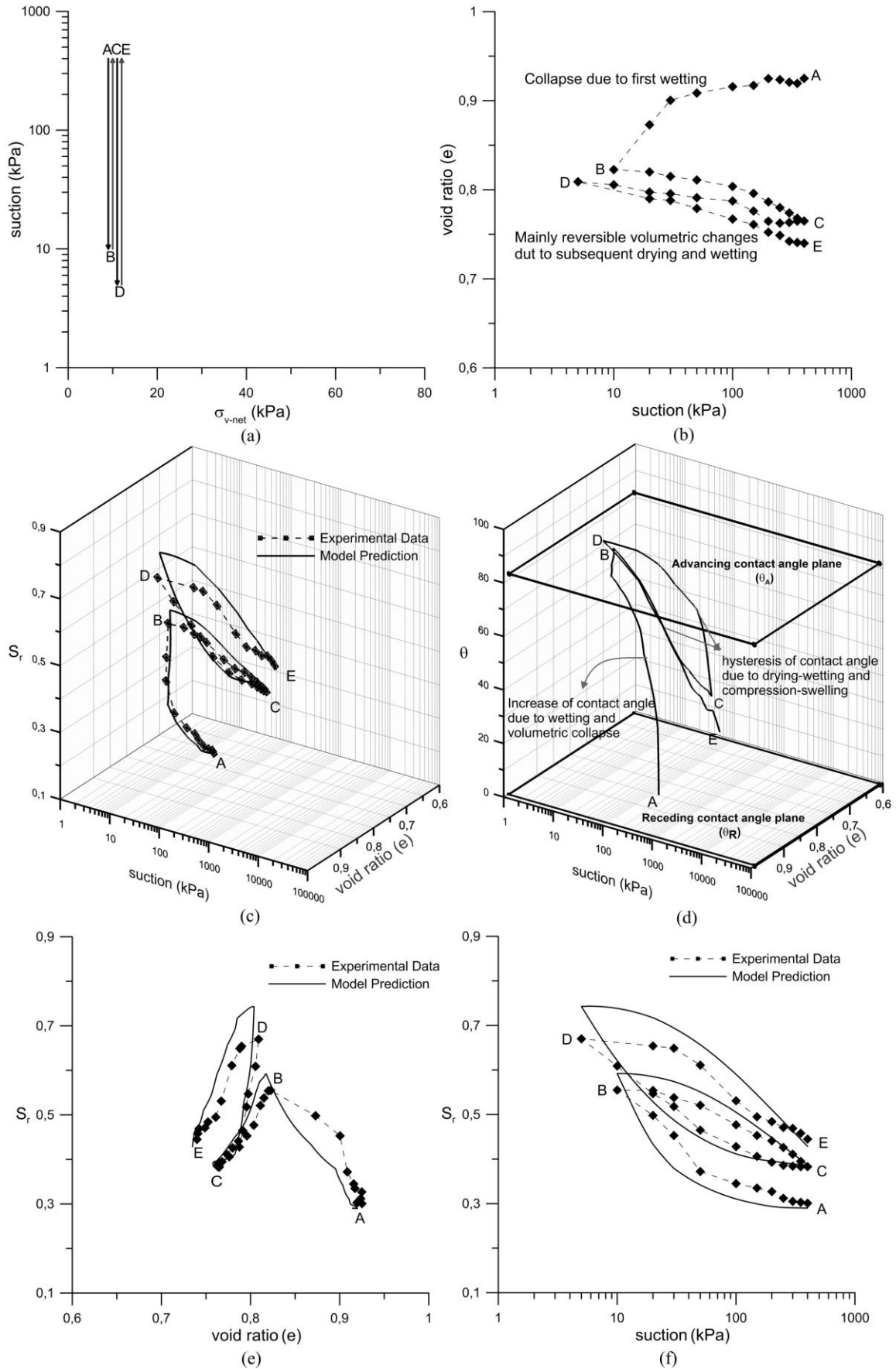
Figure 7. Computed and experimental behaviour during wetting–drying cycles at constant axial net stress (a) applied loading path (b) void ratio-suction data(c) degree of saturation-suction-void ratio data and predictions (d) evolution of the contact angle with suction and void ratio (e) degree of saturation-void ratio data and predictions (f) degree of saturation-suction data and predictions.

5.4 TEST Oe-LU-CW AND MODEL PREDICTIONS

In the last test, the sample was subjected to loading-unloading cycles at constant water content (Oe-LU-CW test). The dry density and the water content of the sample at preparation were 1370 kg/m^3 and 24%, respectively (corresponding to e_0=1.00 and S_{r0}=0.66). The sample was placed in the oedometer and the suction was increased to 200 kPa, at constant axial net stress σ_{v-net}=10 kPa. After equilibrium was established, the water drainage was closed and the water pressure was measured while the air pressure was kept constant. The sample was then subjected to loading-unloading cycles where the water content remained constant (w=11.8%), as shown in Figure 8 (a). The maximum axial net stress of each cycle was σ_{v-net}=150, 500, 1500 kPa, while the minimum axial net stress of each cycle was σ_{v-net}=10 kPa. The loading-unloading steps were applied very slowly to guarantee that the measured water pressure was in equilibrium with the water pressure acting within the soil sample.

Figure 8 (b) shows the volume change of the sample in terms of void ratio and axial net stress. The sample was mechanically wetted when experiencing volumetric contraction during the increase of the axial net stress, and the measured suction decreased as shown in Figure 8 (c). Conversely, suction increased when the sample was subjected to unloading. The water retention state initially lied very close to the main drying surface and the degree of saturation increased slightly, whereas it approached the main wetting surface at lower suction where the degree of saturation started increasing rapidly.

The unloading path changed the degree of saturation while the water retention state lied inside the scanning domain. However, the scanning paths were reversible and they approached the main wetting surface during subsequent reloading. The predicted suction showed good agreement with the experimental values and the model was able to reproduce the loops induced by loading-unloading paths (Figure 8 (c)). Figure 8 (d) also shows the water retention behaviour in the S_r-s-e space and it demonstrates the increase in the degree of saturation resulting from the reduction in the void ratio, while the corresponding decrease in suction was well predicted by the proposed model.
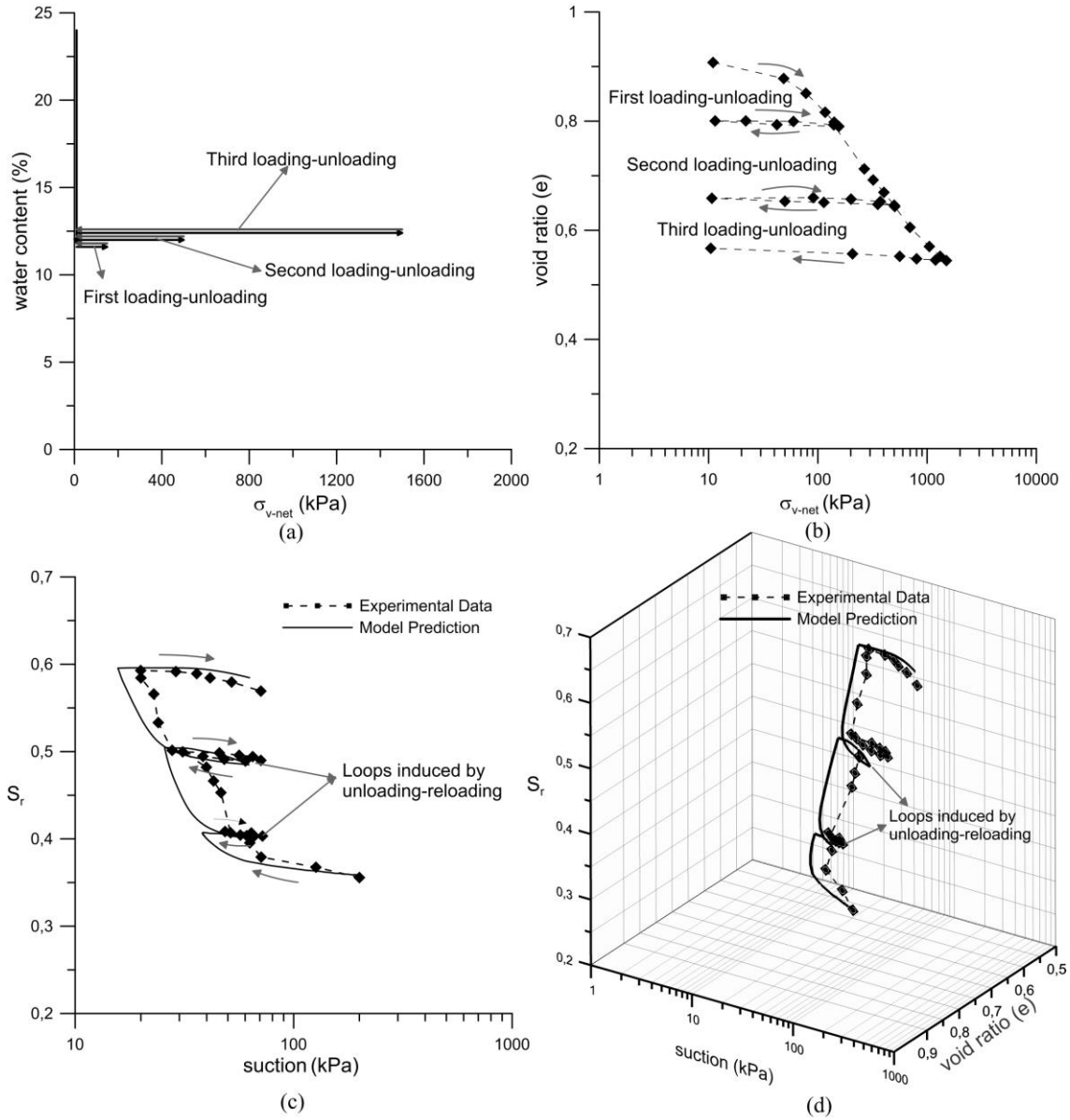
Figure 8. Computed and experimental behaviour during loading-unloading cycles at constant water content
(a) applied loading path (b) void ratio-net stress data (c) degree of saturation-suction data and predictions
(d) degree of saturation-suction-void ratio data and predictions.

6. CONCLUSIONS

The hysteresis associated with the water retention behaviour is not negligible and it has to be taken
into account to properly model the hydro-mechanical behaviour of unsaturated soils. This hysteresis
can be described in terms of contact angle variations. The contact angle changes with suction and
with the volume of the soil, while it can take values between the advancing contact angle (θ_A) and
the receding contact angle (θ_R). The contact angle hysteresis was introduced into a WRM in order

to account for the hysteresis induced by wetting-drying and compression-swelling cycles, in which $\theta=\theta_A$ at the main wetting surface and $\theta=\theta_R$ at the main drying surface.

The model proposed by Gallipoli et al. (2003) was adopted to account for the effects related to void ratio variations, and a differential equation was derived in which two hysteresis functions were proposed to independently reproduce the hysteresis of water retention caused by wetting-drying and compression-swelling cycles. The hysteresis functions were introduced on an empirical basis relying on a conceptual framework which describes the variation of the contact angle with suction and void ratio. However, the proposed framework is open to possible improvements coming from the introduction of different mechanical and hydraulic hysteresis functions obtained by geomechanical or geometrical features of soil-water interface relationships. The proposed WRM is able to reproduce the main wetting and drying surfaces and nonlinear scanning curves in the S_r-s-e space where both mechanical and hydraulic hysteresis of the water retention behaviour can be reproduced.

A series of experimental tests was carried out to study the water retention behaviour of a clayey silt and to investigate the hysteresis induced by wetting-drying and loading-unloading cycles. The proposed model was also used to predict the experimental results after the calibration of only five parameters, which were enough to reproduce the main water retention curves as well as the nonlinear scanning curves. The model predictions, based on the experimental values of void ratio, showed good agreement with the experimental results. The results suggest that the proposed WRM might be coupled efficiently with mechanical models, to properly reproduce the behaviour of unsaturated soils undergoing cyclic hydraulic and mechanical load paths.

REFERENCES

[1] Azizi (2016). PhD Dissertation "effects of repeated hydraulic loads on the microstructure and hydromechanical behaviour of a clayey silt". Politecnico di Milano.

[2] Bachmann JSK, Woche MO. Goebel, (2003). Water Resour. Res. 39. 1353.

[3] Brooks RH, Corey AT. (1964). Hydraulic Properties of Porous Media, Colorado State University.

[4] Campbell GS. (1974). A simple method for determining unsaturated conductivity from moisture retention data. Soil Science 117(6): 311-314.

[5] Chen H, Tang T, Amirfazli A. (2014). Liquid transfer mechanism between two surfaces and the role of contact angles. Soft Matter 10 (15), 2503–2507.

[6] Della Vecchia G, Jommi C, Romero E. (2013). A fully coupled elastic–plastic hydromechanical model for compacted soils accounting for clay activity. International Journal for Numerical and Analytical Methods in Geomechanics 37(5): 503-535.

[7] Di Mundo R, Palumbo F. (2011). Comments regarding an essay on contact angle measurements. Plasma Process Polym, 8(1):14‑18.

[8] Diamantopoulos E, Durner W. (2013). Physically-based model of soil hydraulic properties accounting for variable contact angle and its effect on hysteresis. Advances in Water Resources 59: 169-180.

[9] Eral HB, 't Mannetje DJCM, Oh JM. (2013). Contact angle hysteresis: a review of fundamentals and applications, Colloid and Polymer Science, vol. 291, no. 2, pp. 247–260.

[10] Ethington EF. (1990). Interfacial contact angle measurements of water, mercury, and 20 organic liquids on quartz, calcite, biotite, and Ca-montmorillonite substrates. Rep., USGS, 90-409, 1–18.

[11] Fortes MA. (1982). Axisymmetric Liquid Bridges between Parallel Plates. J. Colloid Interface Sci. 88, 338−352.

[12] Fredlund DG, Xing A. (1994). Equations for the soil-water characteristic curve. Canadian Geotechnical Journal 31(4): 521-532.

[13] Gallipoli D. (2012). A hysteretic soil-water retention model accounting for cyclic variations of suction and void ratio. Géotechnique 62(7): 605-616.

[14] Gallipoli D, Wheeler SJ, Karstunen M. (2003). Modelling the variation of degree of saturation in a deformable unsaturated soil. Géotechnique 53(1): 105-112.

[15] Gan, Y, Maggi F, Buscarnera G, Einav I. (2013). A particle-water based model for water retention hysteresis. Géotechnique letters 3:152-161.

[16] Gao L, McCarthy TJ. (2006). Contact Angle Hysteresis Explained. Langmuir 22(14): 6234-6237.

[17] Gardner, WR. (1958). Some steady-state solutions of the unsaturated moisture flow equation with application to evaporation from a water table. Soil Science 85(4): 228-232.

[18] Hillel D. (1998). Environmental Soil Physics, Elsevier Science.

[19] Hong SJ, Chou TH, Chan SH, Sheng YJ, Tsao HK. (2012). Droplet Compression and Relaxation by a Super hydrophobic Surface: Contact Angle Hysteresis. Langmuir, 28, 5606−5613.

[20] Johnson RE, Dettre RH. (1964). Contact Angle Hysteresis. III. Study of an Idealized Heterogeneous Surface. The Journal of Physical Chemistry 68(7): 1744-1750.

[21] Jommi C. (2000). Remarks on the constitutive modelling of unsaturated soils. Experimental evidence and theoretical approaches in unsaturated soils. Balkema, Rotterdam: 139-153.

[22] Khalili N, Habte M, Zargarbashi S. (2008). A fully coupled flow deformation model for cyclic analysis of unsaturated soils including hydraulic and mechanical hysteresis. Computers and Geotechnics 35(6): 872-889.

[23] Krumpfer JW, McCarthy TJ. (2010). Contact angle hysteresis: a different view and a trivial recipe for low hysteresis hydrophobic surfaces. Faraday Discussions 146(0): 103-111.

[24] Li XS. (2005). Modelling of hysteresis response for arbitrary wetting/drying paths. Computers and Geotechnics 32(2): 133-137.

[25] Liu C, Muraleetharan K. Coupled hydro-mechanical elastoplastic constitutive model for unsaturated sands and silts. i: formulation. International Journal for Numerical and Analytical Methods in Geomechanics 2012;12:239–47.

[26] Longley JE, Dooley E, Givler DM, Napier III WJ, Chaudhury MK, Daniel S. (2012). Drop motion induced by repeated stretching and relaxation on a gradient surface with hysteresis, Langmuir, 28, 13912-13918.

[27] Miller CJ, Yesiller N, Yaldo K, Merayyan S. (2002). Impact of soil type and compaction conditions on soil water characteristic. Journal of Geotechnical and Geoenvironmental Engineering 128: 733‑742.

[28] Mašín D. (2010). Predicting the dependency of a degree of saturation on void ratio and suction using effective stress principle for unsaturated soils. International Journal for Numerical and Analytical Methods in Geomechanics. 34, No. 1, 73–90.

[29] Ng CW, Pang YW. (2000). Influence of stress state on soil-water characteristics and slope stability. Journal of Geotechnical and Geoenvironmental Engineering 126(2):157–166.

[30] Nuth M, Laloui L. (2008). Advances in modelling hysteretic water retention curve in deformable soils. Computers and Geotechnics 35(6): 835-844.

[31] Pedroso DM, Williams DJ. (2010). A novel approach for modelling soil–water characteristic curves with hysteresis. Computers and Geotechnics 37(3): 374-380.

[32] Romero E. (2001). Controlled-suction techniques. Gehling WY, Schnaid F (eds) 4th National Brazilian Symposium on Unsaturated soils. ABMS, Brazil 535-542.

[33] Romero E, Jommi C. (2008). An insight into the role of hydraulic history on the volume changes of anisotropic clayey soils. Water Resources Research 44(5): 1-16.

[34] Romero E, Vaunat J. (2000). Retention curves in deformable clays. In Experimental evidence and theoretical approaches in unsaturated soils (eds A. Tarantino and C. Mancuso), pp. 91–106. Rotterdam: A. A. Balkema.

[35] Rotenberg Y, Boruvka L, Neumann AW. (1984). The shape of nonaxisymmetric drops on inclined planar surfaces. Journal of Colloid and Interface Science 102(2): 424-434.

[36] Salager S, El Youssoufi MS, Saix C. (2010). Definition and experimental determination of a soil-water retention surface. Canadian Geotechnical Journal 47, No. 6, 609–622.

[37] Schwartz LW, Garoff S. (1985). Contact angle hysteresis on heterogeneous surfaces. Langmuir 1(2): 219-230.

[38] Shang J., Flury M., Harsh J.B., Zollars R.L. (2008). Comparison of different methods to measure contact angles of soli colloids. J. Colloid Interface Sci. 328: 299-307.

[39] Sheng D, Zhou AN. (2011). Coupling hydraulic with mechanical models for unsaturated soils. Canadian Geotechnical Journal 48(5): 826-840.

[40] Sun DA, Cui HB, Matsuoka H, Sheng D. (2007). A three-dimensional elastoplastic model for unsaturated compacted soils with hydraulic hysteresis. Soils and foundations 47(2): 253-264.

[41] Tamagnini R. (2004). An extended Cam-clay model for unsaturated soils with hydraulic hysteresis. Géotechnique 54(3): 223-228.

[42] Tarantino A. (2009). A water retention model for deformable soils. Géotechnique 59(9): 751-762.

[43] Tarantino A, De Col S. (2008). Compaction behaviour of clay. Géotechnique 58, No. 3, 199–213.

[44] Tarantino A, Tombolato S. (2005). Coupling of hydraulic and mechanical behavior in unsaturated compacted clay. Géotechnique 55:307–317.

[45] Tsiampousi A, Zdravkvic L, Potts DM. (2013). A three-dimensional hysteretic soil-water retention curve. Géotechnique 63(2): 155-164.

[46] Van Genuchten MT. (1980). A closed-form equation for predicting the hydraulic conductivity of unsaturated soils. Soil science society of America journal 44(5): 892-898.

[47] Vanapalli SK, Fredlund DG, Pufahl DE. (1999). The influence of soil structure and stress history on the soil–water characteristics of a compacted till. Géotechnique 49(2): 143-159.

[48] Vaunat J, Romero E, Jommi C. (2000). An elastoplastic hydromechanical model for unsaturated soils Experimental evidence and theoretical approaches in unsaturated soils: 121-138.

[49] Wheeler SJ, Sharma RS, Buisson MSR. (2003). Coupling of hydraulic hysteresis and stress–strain behaviour in unsaturated soils. Géotechnique 53(1): 41-54.

[50] Song Y, Lu TH. (2012). Study of Soil-Water Characteristic Curve Using Microscopic Spherical Particle Model. Pedosphere 22(1): 103-111.

[51] Zhou A. (2013). A contact angle-dependent hysteresis model for soil–water retention behaviour. Computers and Geotechnics 49: 36-42.

[52] Zhou A, Sheng D. (2015). An advanced hydro-mechanical constitutive model for unsaturated soils with different initial densities. Computers and Geotechnics 63: 46-66.

[53] Zhou A, Sheng D, Carter JP. (2012). Modelling the effect of initial density on soil-water characteristic curves. Géotechnique 62(8): 669-680.

[54] Zhou A, Sheng D, Sloan S, Gens A. (2012). Interpretation of unsaturated soil behaviour in the stress-saturation space, i: volume change and water retention curve. Computers and Geotechnics 43:178–87.

Appendix A

The contact angle between soil particles and water has been rarely measured and examined in the literature. However, the hysteresis of the contact angle is known to be an important feature of water droplet interaction with various solid surfaces. Different methods such as the captive bubble, evaporation technique, sessile drop, and Wilhelmy technique have been used to measure the contact angle (e.g. Di Mundo et al., 2011; Eral et al., 2013). Irreversible changes in the contact angle have been also reported due to the behaviour of a liquid bridge when it is compressed and stretched between two solid surfaces (Figure A-1) (e.g. Fortes, 1982; Hong et al., 2012; Longley et al. 2012, Chen et al., 2014). Different advancing and receding contact angles can be measured, depending on the roughness and the heterogeneity of the solid surface. Figure A-2 shows the variation of the contact angle between a water droplet and an acrylic glass surface when the droplet was repeatedly stretched (the distance between the surfaces (d) increased) and compressed (d decreased), as reported by Hong et al. (2012). During the first compression process, the contact angle was the advancing contact angle (pinning, $\theta = \theta_A \approx 72$) whereas θ decreased during the first stretching process (slipping). At the beginning of the following compression stages, the contact angle increased again to θ_A in the slipping regime and remained constant for further compression. However, θ decreased to $\theta_R \approx 51$ during the last two cycles and remained equal to the receding contact angle for further stretching. This indicates that the values of the contact angles at the surfaces are not necessarily constant but can change between their advancing and receding values. Similarly, pinning and slipping can be also explored during compression and stretching of two spherical solid particles, replicating soil volume changes during compression and swelling, as shown in Figure 2 (b) in the main text by bringing the soil particles closer together or moving them apart, respectively.
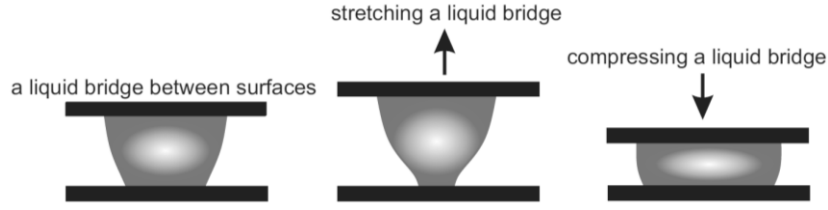
Figure A-1. Schematic of compressing and stretching a liquid bridge between two surfaces.
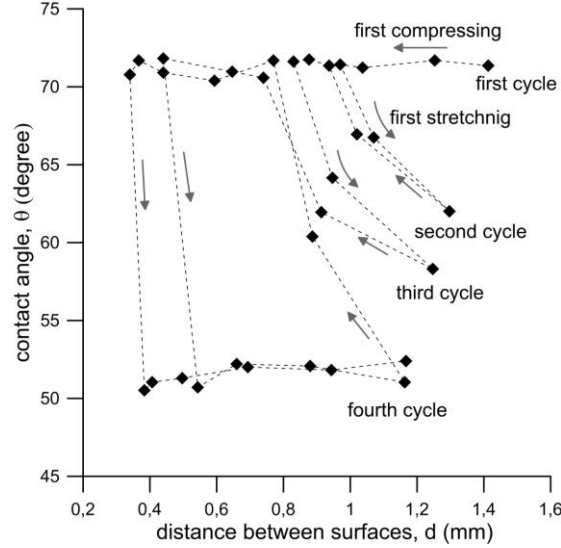

Figure A-2. Changes in the contact angle due to repeated compressing−stretching
(redrawn from Hong et al., 2012).

Appendix B

When the water retention lies on the main wetting surface, the contact angle is the advancing

contact angle ($\theta=\theta_A$). This implies that both $H_\theta{}^e$ and $H_\theta{}^s$ are 0. Therefore, changes in the degree of

saturation $\dot{S}_r$ with respect to Eq. (25) is predicted by

$$\dot{S}_r = \frac{\phi}{s}\dot{s} + \alpha\frac{\phi}{e}\dot{e} \tag{B-1}$$

where $\phi = -mn(\frac{ae^\alpha s\,cos\theta_R}{cos\theta_A})^n \left[1 + (\frac{ae^\alpha s\,cos\theta_R}{cos\theta_A})^n\right]^{-m-1}$.

The above incremental equation is the rate form of Eq. (14) while $\dot{\theta}=0$ and $\theta=\theta_A$. Therefore, S_r on

the wetting branch is obtained by:

$$S_r = \left[1 + (\frac{ae^\alpha s cos\theta_R}{cos\theta_A})^n\right]^{-m} = \left[1 + (\frac{1}{\omega_{ae}}[\frac{cos\theta_R}{cos\theta_A}]s)^n\right]^{-m} \tag{B-2}$$

This equation reminds the van Genuchten model while the effect of the air-entry value (ω_{ae}) is not

expressed by $1/\omega_{ae}=ae^\alpha$ only (Gallipoli's model) but it is also weighted by $cos\theta_R/cos\theta_A$.

32

If we assume that the wetting branch of the water retention curve can be reproduced by the van Genuchten model accounting for the effect of hysteresis only on the air-entry value (while n and m remain constant), S_r can be expressed as below:

$$S_r = \left[1 + (\frac{1}{\omega_{ao}}s)^n\right]^{-m} \tag{B-3}$$

where ω_{ao} is the air-occlusion value.

Considering equation (B-2) and (B-3),

$$\left[1 + (\frac{1}{\omega_{ae}}[\frac{cos\theta_R}{cos\theta_A}]s)^n\right]^{-m} = \left[1 + (\frac{1}{\omega_{ao}}s)^n\right]^{-m} \tag{B-4}$$

Assuming $\theta_R=0$, the relationship between the advancing contact angle and the air-entry and air-occlusion values can be derived:

$$\frac{\omega_{ao}}{\omega_{ae}} = cos\theta_A \tag{B-5}$$

Supplementary Note

Title: A water retention model accounting for the hysteresis
induced by hydraulic and mechanical wetting-drying cycles
Authors: Arash Azizi, Cristina Jommi and Guido Musso

Thanks for your corrections on the language of the manuscript. Those corrections were made and the revised parts are given below. The whole manuscript was also revised carefully to avoid any grammar or syntax error.

Revised manuscript:
Page 9:
Experimental evidence of such irreversible changes in the contact angle was reported looking into the behaviour of a liquid bridge being compressed and stretched between two solid surfaces (Fortes, 1982; Hong et al., 2012; Longley et al. 2012, Chen et al., 2014). The results showed that the contact line can expand or shrink, or remain pinned during compressing and stretching the liquid bridge while the contact angles at the surfaces can change between their advancing and receding values (for details see Appendix A).

Appendix A:
The contact angle between soil particles and water has been rarely measured and examined in the literature. However, the hysteresis of the contact angle is known to be an important feature of water droplet interaction with various solid surfaces. Different methods such as the captive bubble, evaporation technique, sessile drop, and Wilhelmy technique have been used to measure the contact angle (e.g. Di Mundo et al., 2011; Eral et al., 2013). Irreversible changes in the contact angle have been also reported due to the behaviour of a liquid bridge when it is compressed and stretched between two solid surfaces (Figure A-1) (e.g. Fortes, 1982; Hong et al., 2012; Longley et al. 2012, Chen et al., 2014). Different advancing and receding contact angles can be measured, depending on the roughness and the heterogeneity of the solid surface. Figure A-2 shows the variation of the contact angle between a water droplet and an acrylic glass surface when the droplet was repeatedly stretched (the distance between the surfaces (d) increased) and compressed (d decreased), as reported by Hong et al. (2012). During the first compression process, the contact angle was the advancing contact angle (pinning, $\theta=\theta_A\approx72$) whereas θ decreased during the first stretching process (slipping). At the beginning of the following compression stages, the contact angle increased again to θ_A in the slipping regime and remained constant for further compression. However, θ decreased to $\theta_R\approx51$ during the last two cycles and remained equal to the receding contact angle for further stretching. This indicates that the values of the contact angles at the surfaces are not necessarily constant but can change between their advancing and receding values. Similarly, pinning and slipping can be also explored during compression and stretching of two spherical solid particles, replicating soil volume changes during compression and swelling, as shown in Figure 2 (b) in the main text by bringing the soil particles closer together or moving them apart, respectively.
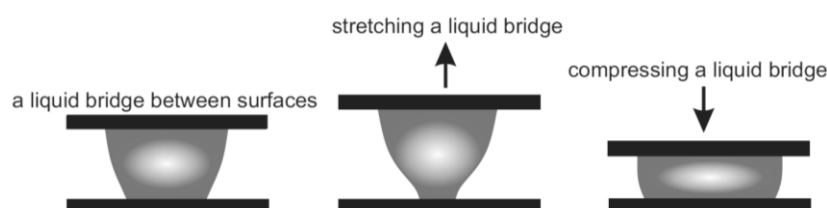

Figure A-1. Schematic of compressing and stretching a liquid bridge between two surfaces.
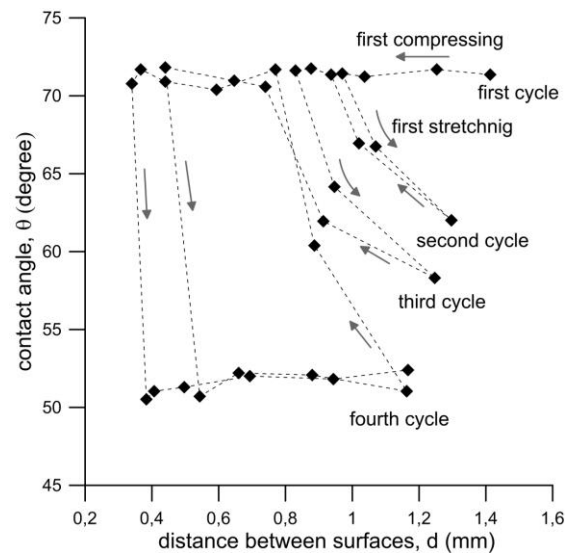
Figure A-2. Changes in the contact angle due to repeated compressing−stretching (redrawn from Hong et al., 2012).